The EMBO Journal (2010) 29, 3249–3259 | © 2010 European Molecular Biology Organization | All Rights Reserved 0261-4189/10
www.embojournal.org

THE EMBO JOURNAL

Molecular basis for activation of G protein-coupled receptor kinases

Cassandra A Boguth[1,3], Puja Singh[1,3,4], Chih-chin Huang[1] and John JG Tesmer[1,2,*]

[1]Life Sciences Institute, The University of Michigan, Ann Arbor, MI, USA and [2]Department of Pharmacology, The University of Michigan, Ann Arbor, MI, USA

G protein-coupled receptor (GPCR) kinases (GRKs) selectively recognize and are allosterically regulated by activated GPCRs, but the molecular basis for this interaction is not understood. Herein, we report crystal structures of GRK6 in which regions known to be critical for receptor phosphorylation have coalesced to stabilize the kinase domain in a closed state and to form a likely receptor docking site. The crux of this docking site is an extended N-terminal helix that bridges the large and small lobes of the kinase domain and lies adjacent to a basic surface of the protein proposed to bind anionic phospholipids. Mutation of exposed, hydrophobic residues in the N-terminal helix selectively inhibits receptor, but not peptide phosphorylation, suggesting that these residues interact directly with GPCRs. Our structural and biochemical results thus provide an explanation for how receptor recognition, phospholipid binding, and kinase activation are intimately coupled in GRKs.

The EMBO Journal (2010) **29,** 3249–3259. doi:10.1038/emboj.2010.206; Published online 20 August 2010
Subject Categories: signal transduction; structural biology
Keywords: crystallography; G protein-coupled receptors; protein kinases; regulation; signal transduction

Introduction

G protein-coupled receptor (GPCR) kinases (GRKs) belong to the protein kinase A, G, and C (AGC) family, and phosphorylate Ser/Thr residues in the cytoplasmic loops and tails of activated GPCRs. Receptor phosphorylation triggers a cascade of events that includes the recruitment of arrestins, uncoupling of GPCRs from heterotrimeric G proteins, receptor internalization, and activation of G protein-independent signal transduction pathways (Pitcher *et al*, 1998; Premont and Gainetdinov, 2007). Although GRKs have a crucial function in desensitization, maladaptive GRK activity is implicated in a range of human diseases, including heart failure and opiate addiction (Pitcher *et al*, 1998; Metaye *et al*, 2005; Dorn, 2009). GRKs are, therefore, considered important therapeutic targets (Metaye *et al*, 2005; Premont and Gainetdinov, 2007; Dorn, 2009).

Similar to heterotrimeric G proteins and arrestins, GRKs are able to discriminate between active and inactive GPCRs. The molecular basis for how these protein families can identify the activated state of almost any GPCR, despite their great sequence divergence, is not well understood. Various biophysical studies have predicted that as a receptor progresses towards its fully active state, the cytoplasmic surface of the GPCR expands and reorganizes to form a binding site for its cellular partners (Rosenbaum *et al*, 2009). For example, in the recent crystal structure of opsin, a GPCR with low constitutive activity, an amphipathic helical peptide derived from the C-terminus of transducin ($G\alpha_t$–Ct) binds directly to a small cavity formed by an outward twist of the third cytoplasmic loop of the receptor (Scheerer *et al*, 2008). Because GRK activity is stimulated by agonist-occupied GPCRs (Onorato *et al*, 1991; Palczewski *et al*, 1991; Chen *et al*, 1993; Kim *et al*, 1993; McCarthy and Akhtar, 2002), GRKs are believed to have, in addition to the canonical phosphoacceptor-binding site in the kinase domain, a receptor docking site that allosterically promotes kinase activity. This docking site may take advantage of the same cavity recognized by $G\alpha_t$–Ct. A molecular understanding of the receptor docking site of GRKs could, therefore, provide significant insight into not only the molecular basis for allosteric activation of GRKs, but also the conformation and properties of activated GPCRs.

Atomic structures for three of the seven vertebrate GRKs have been reported (GRK1, GRK2, and GRK6), representing each of the three vertebrate GRK subfamilies (Lodowski *et al*, 2003, 2006; Singh *et al*, 2008). In each case, the small (or N) and large (or C) lobes of the kinase domain form interfaces with the terminal and bundle lobes, respectively, of a regulator of G protein signalling homology (RH) domain (Figure 1A). In none of the previously determined structures does the kinase domain adopt a 'closed', active conformation similar to the transition-state-like structure of protein kinase A (PKA), wherein ATP and the catalytic machinery are properly aligned with the phosphoacceptor peptide-binding site (Madhusudan *et al*, 2002). Moreover, two structural elements known to be critical for receptor phosphorylation were either not fully ordered or not in a physiologically relevant conformation. The first element is the highly conserved N-terminus (residues 1 to ~20), which is unique to the GRK family of kinases. Truncation of the N-terminus leads to nearly complete loss of receptor phosphorylation (Yu *et al*, 1999; Noble *et al*, 2003; Huang *et al*, 2009), and the binding of recoverin (Chen *et al*, 1995) or an antibody (Palczewski *et al*, 1993) to this region in GRK1 blocks phosphorylation of light-activated rhodopsin. The second element is the AGC kinase carboxyl-terminal tail (C-tail), an extension of the canonical protein kinase domain that has a

*Corresponding author. Life Sciences Institute, The University of Michigan, 210 Washtenaw Avenue, Ann Arbor, MI 48109, USA.
Tel.: +1 734 615 9544; Fax: +1 734 763 6492;
E-mail: tesmerjj@umich.edu
[3]These authors contributed equally to this work
[4]Present address: WM Keck Structural Biology Laboratory, Cold Spring Harbor Laboratory, 1 Bungtown Road, Cold Spring Harbor, NY 11724, USA

Received: 4 May 2010; accepted: 28 July 2010; published online: 20 August 2010

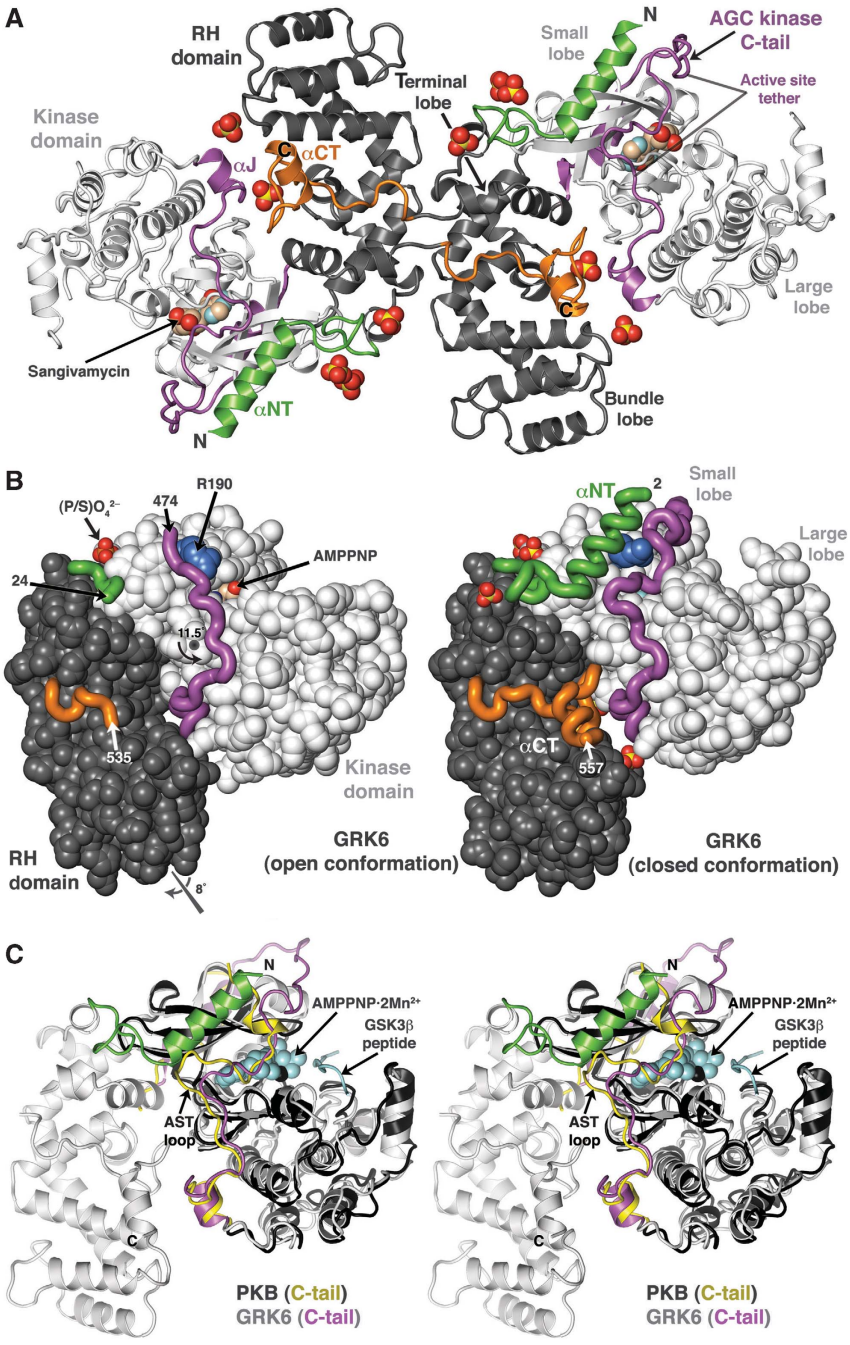

Figure 1 Structure of the GRK6 · sangivamycin complex. (**A**) The GRK6 · sangivamycin dimer. As in prior crystal structures of GRK1 and GRK6, the extreme C-termini form a non-physiological domain swap in the crystal lattice. The N-terminal 18 amino acids (green) of the enzyme form a helix (αNT) whose C-terminal end packs between a region of the small lobe previously identified as being important for GPCR phosphorylation (Huang *et al*, 2009) and the AGC kinase C-tail (magenta). The C-terminus of GRK6 (orange) winds between the RH (grey) and kinase (white) domains and ends in an amphipathic helix (αCT) that docks between the RH and kinase domains. Sangivamycin and sulphate ions are shown as sphere models with carbons coloured tan, nitrogens cyan, oxygens red, and sulphurs yellow. The same colour scheme is used for GRK6 and ligands in all subsequent figures, unless otherwise indicated. (**B**) The kinase domain of the GRK6 · AMPPNP complex (left, PDB entry 2ACX) is more open and less ordered than that of the GRK6 · sangivamycin complex (right). The orientation is the same as the right-most subunit in panel **A**, with the C-terminal domain-swapped region of the second chain mapped back on the subunit. The GRK6 · AMPPNP complex was positioned by superimposing its small lobe with that in the sangivamycin complex. Both GRK6 structures are shown as sphere models except for the N-terminus, C-tail, and C-terminal regions, which become better ordered as the kinase domain progresses to a more closed conformation (right). Numbers indicate the amino-acid number at the ends of each ordered segment of the polypeptide chain. Arg190, a residue previously shown to be critical for receptor and peptide phosphorylation (Huang *et al*, 2009), is coloured blue. A common divalent anion-binding site was observed in each structure. A 11.5° rotation of the large lobe around an axis oriented out of the page, as indicated, is required to superimpose the large lobe of the GRK6 · AMPPNP complex with that of the GRK6 · sangivamycin complex. An 8° clockwise rotation of the bundle subdomain of the RH domain, around the axis indicated (bottom left), also occurs upon transition to the more closed state. (**C**) Stereo view of the closed states of GRK6 (light grey) and protein kinase B (PKB, black). The two AGC kinases were superimposed using their small lobes, showing that their large lobes are in a similar, relatively closed configuration. The AMPPNP ligand and glycogen synthase kinase 3β (GSK3β) peptide (cyan) are from the structure of PKB (PDB entry 1O6L). The PKB C-tail (yellow) has a longer AST loop that interacts with the same region of the small lobe as the C-terminal end of αNT in GRK6 (Figure 2).

regulatory function in AGC kinases and that becomes increasingly well ordered as the kinase approaches its active conformation (Kannan *et al*, 2007). The central segment of the C-tail, known as the 'active site tether' (AST), passes over the active site of the kinase domain and contains residues known to be important for GRK activity (Huang *et al*, 2009; Sterne-Marr *et al*, 2009).

Herein, we present new structures of GRK6 in a relatively closed conformation, wherein both the N-terminus and C-tail are well ordered and interact in a manner that is consistent with their anticipated functions in stabilizing the active form of the enzyme and in forming a docking site for activated GPCRs. We also provide biochemical evidence that residues at the extreme N-terminus of GRK6 interact directly with receptors. These results allow generation of a model of the GRK–GPCR complex that helps to explain how receptor and phospholipid binding cooperatively stabilize the active state of GRKs, and how GRKs are able to selectively recognize the activated state of a GPCR.

Results

Structure of GRK6 in a closed conformation

We crystallized a palmitoylation-deficient mutant of human GRK6 in complex with either the adenosine analogue sangivamycin or AMP, and collected anisotropic diffraction data to 2.7 and 2.9 Å spacings, respectively (Table I). As in prior crystal structures of GRK6 and GRK1, the protein crystallized as a dimer with a C-terminal domain swap forming part of the two-fold interface (Figure 1A). However, strikingly different from prior GRK structures, all of the regions known to be critical for the phosphorylation of active GPCRs are ordered, including the extreme N-terminus and the AST region of the C-tail (Figure 1B), and have coalesced to stabilize the kinase domain in a novel, relatively closed conformation. An additional 22 amino acids at the C-terminus also become ordered (Figure 1B). Relative to the previously determined GRK6·adenylyl-imidodiphosphate (AMPPNP) structure (Lodowski *et al*, 2006), the large lobe of the kinase domain is rotated 11.5° towards the small lobe, severing its interactions with the bundle lobe of the RH domain. In addition, the bundle lobe of the RH domain has rotated ~8° relative to its terminal lobe (Figure 1B). Although an additional ~7° rotation of the large lobe is still required for the kinase domain to adopt a conformation similar to the active states of PKA (Madhusudan *et al*, 2002) or protein kinase B (PKB) (Yang *et al*, 2002) (Figure 1C), the GRK6·sangivamycin/AMP structures represent the most complete and closed structures of a GRK determined to date. Full domain closure may require the binding of ATP and/or GPCRs.

An N-terminal helix stabilizes the closed conformation of GRK6

Residues 2–18 of the GRK N-terminus form a single α helix (αNT) that makes extensive interactions with conserved residues in both the small lobe and C-tail known to be

Table I Crystallographic data and refinement statistics

Ligand (PDB entry): X-ray source:	Sangivamycin (3NYN) APS beam line 21 ID-G	AMP (3NYO) APS beam line 21 ID-G
Wavelength (Å)	0.97856	0.97856
D_{min} (Å)	2.7 (outer shell: 2.75–2.7)	2.9 (outer shell: 2.95–2.9)
Space group	$P6_1$	$P6_1$
Cell constants (Å; deg)	$a=b=154.6$, $c=207.9$; $\alpha=\beta=90$, $\gamma=120$	$a=b=154.6$, $c=208.1$; $\alpha=\beta=90$, $\gamma=120$
Unique reflections	77 021 (3771)	61 817 (3071)
Unique reflections (ellipsoidal cutoff)[a]	45 850 (47)	34 428 (39)
Average redundancy	3.8 (3.1)	4.5 (4.4)
Average redundancy (ellipsoidal cutoff)[a]	3.9 (4.8)	4.4 (4.3)
R_{sym} (%)	9.9 (>100)	11.6 (>100)
R_{sym} (%; ellipsoidal cutoff)[a]	8.8 (35.1)	10.8 (45.5)
Completeness (%)	99.9 (99.8)	100 (100)
Completeness (%; ellipsoidal cutoff)[a]	59.4 (1.2)	55.7 (1.3)
$\langle I\rangle/\langle\sigma_I\rangle$	9.7 (0.21)	6.5 (0.21)
$\langle I\rangle/\langle\sigma_I\rangle$ (ellipsoidal cutoff)[a]	19 (3.8)	15 (2.4)
Refinement resolution (Å)	30–2.7 (outer shell: 2.8–2.7)	30–2.9 (outer shell: 3.0–2.9)
Total reflections used	45 750 (154)	34 329 (109)
Protein atoms	8908	8908
Non-protein atoms	138	131
RMSD bond lengths (Å)	0.008	0.007
RMSD bond angles (deg)	1.0	1.0
Estimated coordinate error (Å)	0.20	0.27
Average B-factor (Å^2)[b]	77	100
Ramachandran plot statistics		
Most favoured, disallowed (%)	88.0, 0.0	86.1, 0.0
R_{work}	20.1 (29.8)	21.0 (36.6)
R_{free}[c]	23.6 (36.8)	25.3 (31.3)
R_{final}[d]	22.7 (49.5)	22.2 (28.2)

[a]Diffraction data extended to 3.5 Å along a^* and b^*, and to 2.7 Å along c^* for the sangivamycin data set, and to 4.0 Å along a^* and b^*, and to 2.9 Å along c* for the AMP data set. Scaling was performed after rejection of observations outside a standard ellipsoid with these reciprocal space dimensions. Table entries that specify an ellipsoidal cutoff are statistics calculated after application of the ellipsoidal cutoff, and thus *R*-factors and completeness are lower for these entries.
[b]*B*-factor does not include the TLS contribution.
[c]5% of the data set was excluded from refinement to calculate R_{free}.
[d]All reflections were used in the final rounds of refinement.

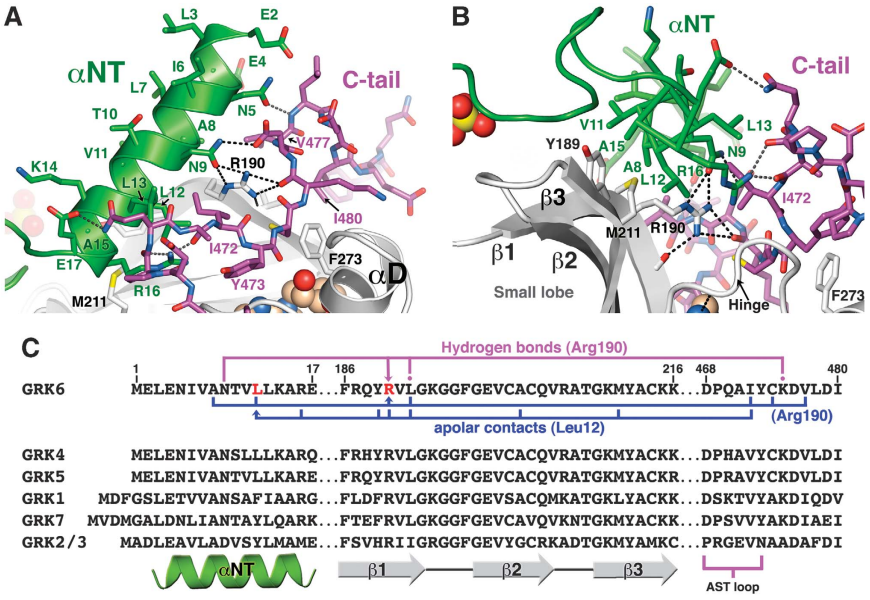

Figure 2 Intramolecular contacts of αNT. (**A**) The αNT helix and C-tail of the kinase domain form bridging interactions between the small and large lobes that stabilize the closed state. Hydrogen bonds between αNT (green) and the C-tail (magenta) are shown as dashed lines. The side chain of Phe273 in αD forms the most significant interaction between the large lobe and the C-tail. Sangivamycin, which occupies the ATP-binding site, and a nearby sulphate ion are shown as spheres. (**B**) The αNT helix is the keystone in an arch of interactions that spans the nucleotide-binding site and hinge region of the kinase domain. The view is directed at the C-terminal end of αNT, which is shown as a Cα trace. The arch begins on the left, as shown, with the small lobe, followed by αNT, then the C-tail, and ends on the right with the αD helix of the large lobe (Phe273). The side chains of Leu12 and Arg190 are adjacent and pack underneath the arch. Mutation of either residue dramatically reduces GPCR and peptide phosphorylation (Table II) and (Huang *et al*, 2009), respectively. (**C**) Interaction network of Leu12 and Arg190 in the context of the GRK primary sequence alignment. Hydrogen bonds mediated by Arg190 are shown with purple connecting lines, and dots indicate bonds involving backbone atoms. Apolar contacts are shown with blue connecting lines. All sequences correspond to the human enzyme.

important for GRK activity against receptor and peptide substrates (Huang *et al*, 2009; Sterne-Marr *et al*, 2009) (Figure 2). Two of these residues, Arg190 in the small lobe and Ile472 in the C-tail, seem to have particularly important structural roles. Arg190 is found in a patch of residues on the surface of the small lobe, relatively distant from the active site, that are uniquely conserved in the GRK subfamily of AGC kinases ('site 1' in Huang *et al*, 2009). However, in prior GRK structures, the residues in this patch were solvent exposed and/or poorly ordered, and thus their function in catalysis was not clear. In the closed structure of GRK6, the aliphatic portion of the Arg190 side chain packs against the side chains of Ala8 and Leu12 in αNT, and its guanidinium group forms bridging hydrogen bonds between the small lobe, the side chain of Asn9 in αNT, and the backbone carbonyl of Lys475 in the C-tail (Figure 2A and C). The extensive contacts of Arg190 are consistent with prior mutagenesis studies. Substitutions at this position with alanine in GRK1, GRK2, and GRK6 resulted in nearly complete loss of kinase activity, and even conservative substitution to lysine in GRK1 was nearly as defective as truncation of the N-terminal 15 amino acids of the enzyme (Huang *et al*, 2009). In the C-tail, the side chain of Ile472 is accommodated in a hydrophobic pocket created by the side chains of Asn9, Leu12, and Leu13 on αNT (Figure 2). Substitution of the residue equivalent to GRK6-Ile472 in GRK1 and GRK2 also resulted in a dramatic loss of kinase activity (Huang *et al*, 2009; Sterne-Marr *et al*, 2009). The extensive contacts of Arg190 and Ile472 and the fact that their substitution leads to diminished activity against both receptor and peptide substrates both suggest that their function is to stabilize the active conformation of GRK6—a state that is likely similar to the closed conformation reported here.

Structure of the AGC kinase C-tail of GRK6

Unlike in previously determined GRK structures, the entire AGC kinase C-tail of GRK6 (residues 452–502) is ordered, in particular the AST region. The AST begins with the 'AST loop', which is formed in GRK6 by a hydrogen bond between the backbone amide of Asp468 and the side chain hydroxyl of Tyr473. The loop is sandwiched between αNT and the large lobe of the kinase domain (Figure 2A and B). In other AGC kinase families, the AST loop is four residues longer and these additional residues become ordered and interact with the small lobe as the kinase domain adopts a more closed conformation (Figure 1C). In GRKs, the loop is too short to form an analogous 'clasp', leaving instead a shallow canyon between the small lobe and C-tail that instead serves as the docking site for the C-terminal end of αNT (Figure 2B). Thus, from a structural standpoint, the C-terminal end of αNT seems to compensate for the shorter AST loops of GRKs by taking on the function of a stabilizing bridge between the small and large lobes.

Two residues after the AST loop, the GRK6 C-tail follows a unique path from those of other characterized AGC kinases (Figures 1C and 2A). Residues 476–479 form a tight turn that provides hydrogen bonds with residues in αNT. Mutation of residues in GRK1 and GRK2 equivalent to GRK6-Ile480, whose side chain packs between this tight turn and the small lobe, results in significant defects in catalytic activity (Huang *et al*, 2009; Sterne-Marr *et al*, 2009). The C-tail then wanders across the small lobe and forms a belt around the αB

helix, whose surface exposed residues form another region uniquely conserved in GRKs ('site 2' in Huang *et al*, 2009; Figure 3A). This latter segment of the C-tail contains the canonical AGC kinase 'turn motif', a site of auto-phosphorylation in some GRKs, but its location and structure is distinct from that of PKA. The GRK6 C-tail ends, as it does in PKB (Yang *et al*, 2002), by contributing a final helix and short β-strand to the small lobe.

Membrane interaction surface of GRK6

The ability of a GRK to phosphorylate a GPCR is almost always dependent on the presence of a negatively charged membrane such as one that contains phosphatidylinositol 4,5-bisphosphate (PIP_2) (Pitcher *et al*, 1996, 1998). Consequently, GRKs are believed to contain structural elements that facilitate their interactions with anionic head groups. An intensely basic, relatively flat surface is found immediately adjacent to the protruding N-terminal end of the αNT helix in GRK6 (Figure 3A and B). Three sulphate anions from the crystallization solution are bound to this surface (Figure 3C). One of these sites was also occupied by a divalent anion in the GRK6 · AMPPNP structure, which was crystallized in the absence of sulphate (Figures 1B and 3C), suggesting that it represents a high-affinity-binding site for PIP_2 (Pitcher *et al*, 1996). Residues involved in coordinating these anions are highly conserved in the GRK4 subfamily, and bulk substitution of six of the N-terminal Arg/Lys residues in this region with alanine ablated PIP_2-dependent receptor phosphorylation in GRK5 (Pitcher *et al*, 1996). Interestingly, in this same study, PIP_2 did not stimulate the phosphorylation of peptide substrates. Considered along with our structural data, this suggests that although the basic region binds directly to the cell membrane, such is still insufficient to stabilize the closed state of the kinase domain.

A putative GPCR docking site

If the aforementioned lipid-binding surface is used to define the plane of the lipid bilayer when GRK6 is at the cell membrane (Figure 3), then the N-terminal end of αNT would protrude into the plane of the membrane. Exposed hydrophobic residues at the N-terminal end of αNT (Leu3, Ile6, Val7, Thr10, and Val11) form a continuous hydrophobic surface that could favourably interact with the hydrophobic phase of the bilayer (Figures 2A and 3A). However, the presence of two negatively charged residues at the N-terminus of αNT in most GRKs (Glu2 and Glu4 in GRK6; Figure 2C) argues against αNT serving as a membrane-binding element. The highly conserved nature of residues that form this hydrophobic surface (Figure 2A and C) is more consistent with these residues comprising a functionally important interaction site, such as one that might be formed with an activated GPCR. In the crystal lattice, this hydrophobic surface forms a short, anti-parallel coiled–coil interaction with the same surface of a non-crystallographically related αNT helix. This strong lattice contact likely plays a similar role as an activated GPCR in that it stabilizes the αNT helix and, consequently, the closed state of GRK6.

Mutational analysis of the GPCR docking site

If the αNT helix were important for direct interactions with active receptors, then site-directed mutation of the exposed hydrophobic residues in αNT should inhibit phosphorylation

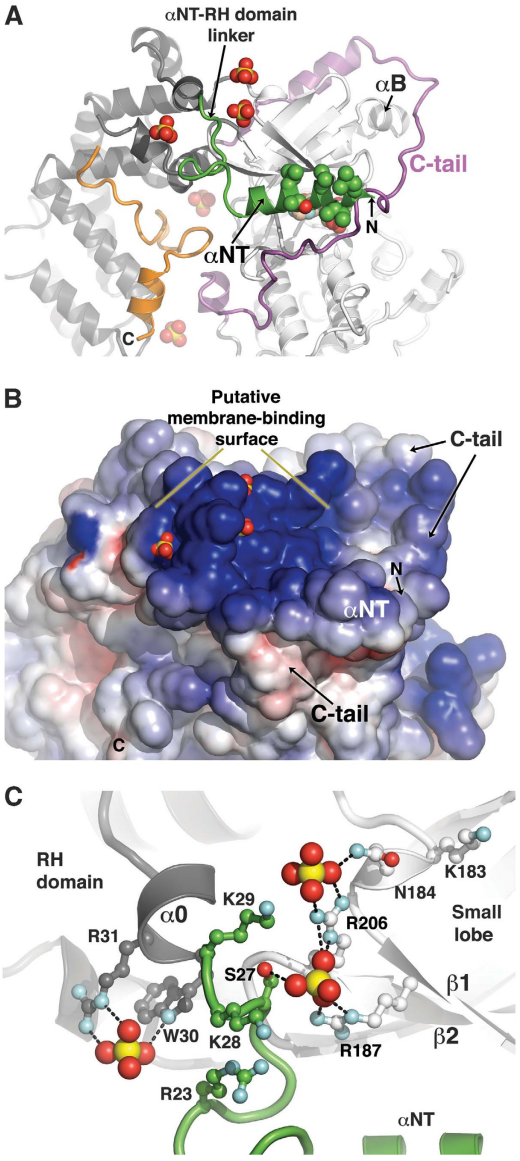

Figure 3 Membrane interacting surface of GRK6 in its closed conformation. (**A**) The expected membrane interacting surface of GRK6. The view is from the perspective of the proposed phospholipid bilayer. Three sulphate anions, which may correspond to binding sites for phosphate groups in PIP_2, bind to a relatively flat region formed by residues 23–31 of the linker joining αNT and the RH domain and by adjacent regions of the small lobe. Next to this region, the N-terminal end of αNT projects into the expected plane of the lipid bilayer and bears conserved, exposed hydrophobic residues (green spheres). (**B**) Molecular surface of GRK6 coloured by its electrostatic potential. The view is the same as in panel **A**. The surface is coloured in a gradient from $\leqslant -6\,kT/e^-$ (red, acidic) to $\geqslant 6\,kT/e^-$ (blue, basic). The relatively flat region next to αNT, which contains the divalent anion-binding sites, is exceptionally basic and thus well suited to directly interact with the negatively charged inner leaflet of the cell membrane. (**C**) Interactions of residues in the proposed membrane binding region of GRK6. All side chains shown are conserved in the GRK4 subfamily of GRKs. The centrally positioned anion was observed in both the AMPPNP (Lodowski *et al*, 2006) and sangivamycin/AMP complexes. Hydrogen bonds are indicated by black dashed lines.

of a GPCR, but not of a short peptide that contains the native phosphoacceptor sites from the same receptor. We, therefore, measured the ability of the GRK6C splice variant (Vatter *et al*, 2005) to phosphorylate bovine rod outer segments (bROS)

Table II Kinetic parameters for bROS and peptide C phosphorylation by GRK6C αNT variants

	bROS phosphorylation		Peptide C phosphorylation	
	k_{cat}/K_M (per μM/h)	Fold decrease (k_{cat}/K_M)	k_{cat}/K_M (per mM/h)	Fold decrease (k_{cat}/K_M)
Wild type	1.7 ± 1	1	0.14 ± 0.10	1
L3A	0.90 ± 0.7	2	0.12 ± 0.09	1
E4A	0.60 ± 0.3	3	0.088 ± 0.005	2
I6A	0.14 ± 0.1	12	0.11 ± 0.01	1
V7A	0.13 ± 0.06	13	0.10 ± 0.06	1
I6A/V7A	0.05 ± 0.004	36	0.14 ± 0.09	1
I6E/V7E	0.0096 ± 0.007	180	0.10 ± 0.01	1
N9A	0.012 ± 0.005	140	0.018 ± 0.007	8
L12A	0.0016 ± 0.0004	1100	0.022 ± 0.02	6
L13A	0.28 ± 0.1	6	0.026 ± 0.002	5

For bROS, values represent mean ± standard error of the linear regression fit calculated from 3 to 6 independent experiments. For peptide C phosphorylation, values shown represent mean ± standard error of the non-linear regression fit calculated from 2 to 4 independent experiments. As the Michaelis–Menten plots are linear for bROS and peptide up to the highest concentration tested (80 μM and 4 mM, respectively), the k_{cat} could not be determined with confidence. Therefore, only k_{cat}/K_M values are provided.

and 'peptide C', which contains the known phosphoacceptor sites from the C-terminus of rhodopsin (Table II). The I6A and V7A mutations exhibited 12–13-fold defects in bROS phosphorylation, but no significant defect in peptide phosphorylation, as predicted by our docking model. The I6A/V7A and I6E/V7E double mutants exhibited 36- and 180-fold defects, respectively, in receptor phosphorylation, a progression consistent with the idea that these residues interact with a hydrophobic surface, such as that provided by IL3 of an activated GPCR. In contrast, residues from αNT that form extensive interactions with the small lobe and C-tail, such as Asn9 and Leu12 (Figure 2), exhibited significant defects in both bROS and peptide phosphorylation, consistent with their proposed function in stabilizing the active conformation of the kinase domain. Our results are also consistent with the defects in receptor phosphorylation reported for other mutants in the N-termini of GRK5 and GRK2, with the exception that we were unable to observe significant defects for mutants of Leu3 and Asp4 in our assays (Yu *et al*, 1999; Noble *et al*, 2003; Pao *et al*, 2009). This difference may simply reflect the fact that different GRKs have different dependencies on each of these residues when they interact with specific GPCRs.

Ligand interactions in the kinase active site

We were able to co-crystallize GRK6 in this relatively closed state in the presence of either sangivamycin or AMP. The ligands bind similarly in the canonical ATP-binding site that is formed between the small and large lobes of the kinase domain, adjacent to the hinge joining the two lobes, and directly underneath the C-tail (Figures 2B and 4). Sangivamycin is a *Streptomyces*-derived adenosine analogue, differing by a 7-deaza-7-carbamoyl substitution, long recognized for its antitumor properties. It is a relatively potent GRK inhibitor (Palczewski *et al*, 1990) and binds to GRK6 with a K_D of ~1 μM, which is about 30-fold tighter than adenosine (data not shown). The 7-carbamoyl substitution packs deep in the GRK active site where it forms van der Waals interactions with the side chains of Ser328 and the 'gatekeeper' residue Leu263 (Figure 4A). Its amide group also forms hydrogen bonds with the side chain of Asp329, a residue that coordinates Mg^{2+} in AGC kinase complexes with ADP or ATP, and with a buried water molecule that also coordinates the backbone amide of Asp329. Sangivamycin can be displaced out of the active site by soaking crystals in the presence of adenine nucleotides (data not shown), suggesting that the GRK C-tail is not acting as a gate to lock ATP or its products in the active site. AMP makes contacts analogous to those of the AMP moieties of ADP or ATP in other AGC kinase structures, with its adenine ring forming two specific hydrogen bonds with backbone atoms in the hinge (Figure 4B). Unlike in PKA, residues in the kinase C-tail make no direct contact with the bound ligands.

Sangivamycin was previously shown to be about five-fold more potent against protein kinase C than PKA (Loomis and Bell, 1988). AGC kinases other than GRKs and most PKC isoforms have bulkier Thr/Val residues at the position equivalent to GRK6-Ser328, which would sterically crowd the 7-carbamoyl group (Figure 4A) and at least partially explain the observed selectivity.

A structural function for the GRK6 C-terminus

The unique C-terminal regions of the three GRK subfamilies (i.e. the region that extends beyond the end of the RH domain) are expected to have functions in membrane targeting and, in at least some cases, allosteric activation (Pitcher *et al*, 1998; Lodowski *et al*, 2005). An additional 22 residues from the C-terminus of GRK6 are ordered in the GRK6·sangivamycin/AMP structures compared with the more open GRK6·AMPPNP complex (Figures 1B and 5). The newly ordered C-terminal residues of GRK6 wind through the cleft formed between the bundle and terminal lobes of the RH domain, and end in an amphipathic helix (αCT, residues 548–557) that bridges the bundle lobe of the RH domain and the αJ region of the kinase domain (Figures 1A, B and 5). Conserved residues in the αCT helix that were previously proposed to interact directly with the cell membrane (Thiyagarajan *et al*, 2004) instead make interactions with conserved regions of the RH and kinase domains that are only possible when the kinase domain adopts its relatively closed conformation. The palmitoylation sites that occur several residues after the end of αCT (a region disordered in this structure) are thus relatively distant from the expected membrane surface (Figures 3 and 6). However, this observation is consistent with the fact that the GRK6C splice variant, which lacks the palmitoylation sites entirely and whose C-terminus is similar to the end of the observed structure reported here, fully retains its ability to bind membranes and phosphorylate activated GPCRs (Vatter *et al*, 2005). Palmitoylation is, therefore, dispensable for function in GRK6, and the region C-terminal to αCT, and its modifications, may chiefly be involved in auto-regulation of the adjacent kinase domain.

Discussion

We have determined new structures of GRK6 in a closed conformation in which structural elements known to be critical for GPCR phosphorylation are fully ordered. These

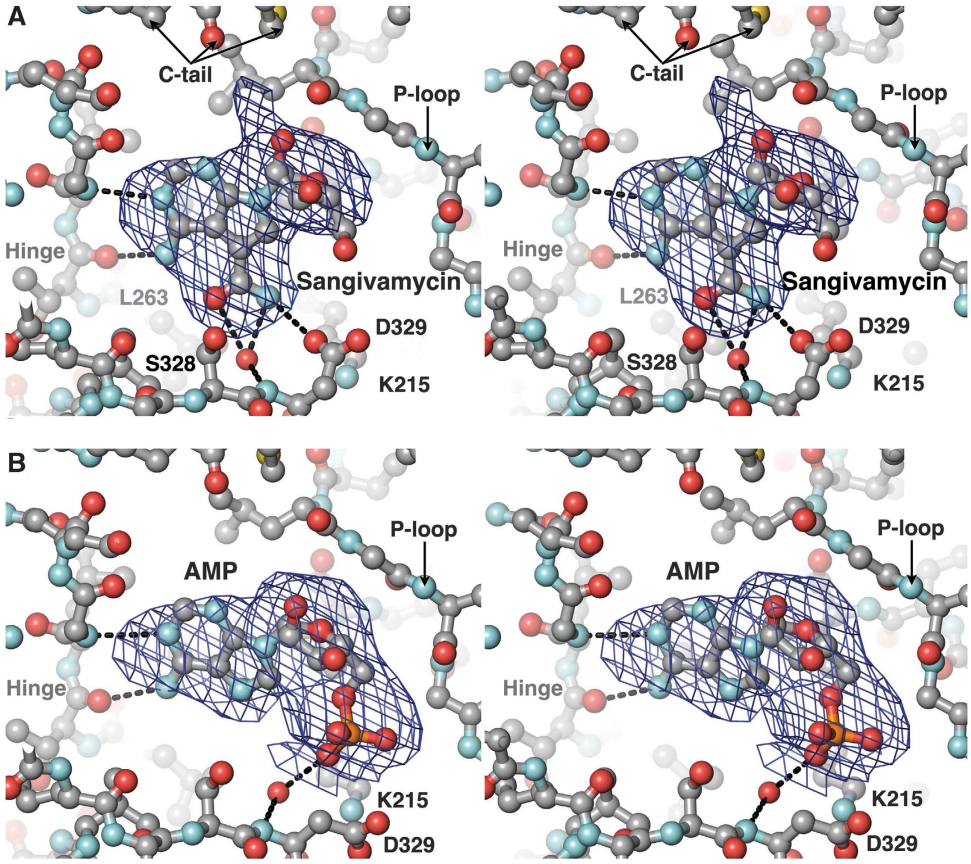

Figure 4 Ligands bound in the active site of GRK6. (**A**) Stereo view of sangivamycin bound to GRK6. The $3\sigma|F_o|-|F_c|$ omit map for sangivamycin is shown as a blue wire cage. The inhibitor is shown as a ball-and-stick model, and hydrogen bonds are depicted by black dashed lines. The 7-deaza-7-carbamoyl substitution of the adenosine analogue forms three specific hydrogen bonds, and packs between the Leu263 and Ser328 side chains. Unlike in other characterized AGC kinases, the C-tail region does not make direct contacts with the bound ligand, which may help explain why nucleotide binding alone does not induce kinase domain closure in GRKs (Lodowski *et al*, 2006; Singh *et al*, 2008). (**B**) Stereo view of AMP bound to GRK6. The electron density shown corresponds to a $3\sigma|F_o|-|F_c|$ omit map for AMP.

elements interact with each other using residues that are uniquely conserved in GRKs and known to be important for kinase activity. In this relatively closed state, the αNT helix is the keystone in a bridge of interactions that begins with the small lobe, followed by the C-terminal end of αNT, then the AGC kinase C-tail, and ends with the αD helix of the large lobe (Figure 2B). The exposed, conserved hydrophobic patch at the N-terminal end of αNT, and its spatial relationship to the proposed membrane-binding surface of GRK6 (Figure 3), strongly suggest that it represents the crux of the docking site for activated GPCRs. The balance of the mutagenesis data that reported here (Table II) and in the literature supports this conclusion. The GRK6·sangivamycin/AMP structures thus represent a conformation that is likely very close to the activated state of the enzyme and that serves as a reasonable model for the activated, GPCR-bound state of all GRKs.

To model how αNT might interact with an activated receptor, we compared the GRK6 structure to the recently reported structure of the opsin·$G\alpha_t$–Ct complex (Scheerer *et al*, 2008). As proposed for the N-terminal end of αNT, the C-terminal end of the C-terminal helix of the heterotrimeric Gα subunit is a major determinant for binding and selective recognition of activated receptors (Oldham and Hamm, 2006). In the opsin·$G\alpha_t$–Ct complex, the fifth and sixth transmembrane spans (TM5 and TM6) of the receptor are twisted outward from the helical core, relative to dark-state rhodopsin, to expose a hydrophobic surface on their inner side to which the amphipathic $G\alpha_t$–Ct helix binds (Scheerer *et al*, 2008). Interestingly, the $G\alpha_t$–Ct helix adopts a similar angle with respect to the proposed membrane plane as the αNT helix of GRK6 (Figures 3 and 6). Although the GRK6 αNT and $G\alpha_t$–Ct helices have opposite orientations, their exposed hydrophobic residues can be superimposed to dock GRK6 with opsin (Figure 6). Features in support of the resulting model are that (1) it places both IL3 and the C-terminus of the GPCR, either of which can be phosphorylated by GRKs provided sufficient length, within easy reach of the active site cleft in the kinase domain; (2) it would readily accommodate the variable lengths of IL3 that are found in GPCRs; and (3) it provides an explanation for why both anionic phospholipids and activated GPCRs are required for GRK activity, as follows. GRKs are not very selective for any given GPCR, but are selective for activated receptors. There are, accordingly, no specific hydrogen bonds or packing interactions predicted by our docking model, and the direct interaction of αNT with the receptor is consequently of relatively low affinity. Cooperative interaction of the GRK with both activated receptor and anionic lipids is thus required to achieve enough affinity to stabilize the closed, active conformation of the GRK, which is complementary in

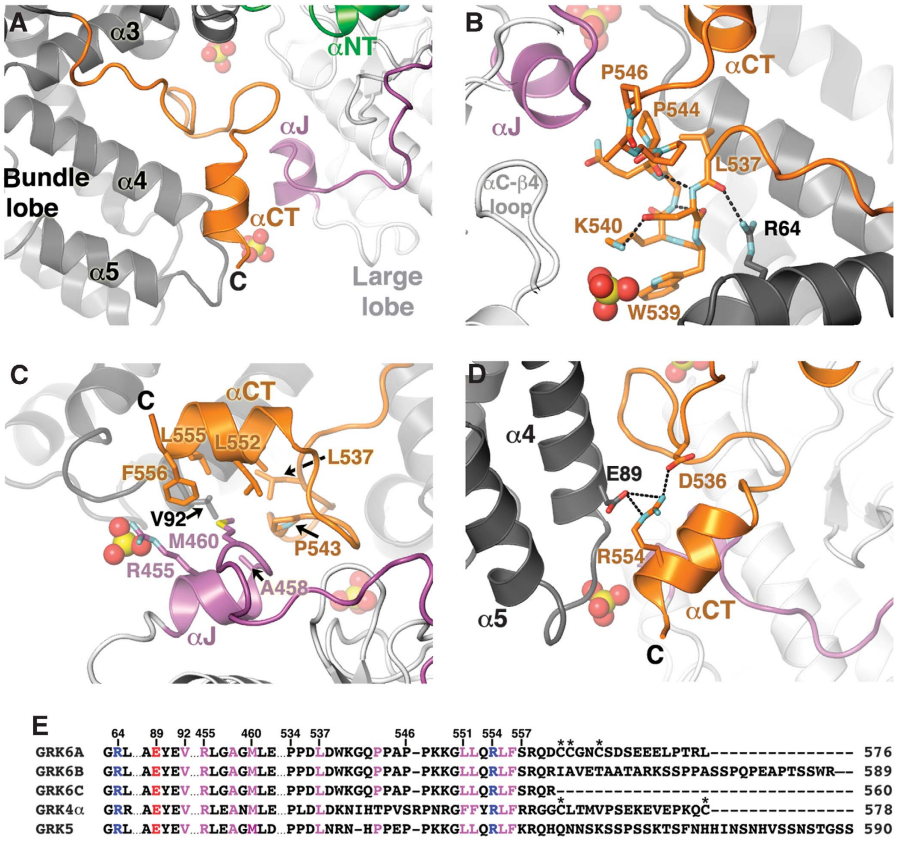

E

```
                 64   89  92 455    460   534 537          546      551 554 557
GRK6A   GRL..AEYEV..RLGAGMLE..PPDLDWKGQPPAP-PKKGLLQRLFSRQDCCGNCSDSEEELPTRL---------- 576
GRK6B   GRL..AEYEV..RLGAGMLE..PPDLDWKGQPPAP-PKKGLLQRLFSRQRIAVETAATARKSSPPASSPQPEAPTSSWR-- 589
GRK6C   GRL..AEYEV..RLGAGMLE..PPDLDWKGQPPAP-PKKGLLQRLFSRQR---------- 560
GRK4α   GRR..AEYEV..RLEANMLE..PLDLDKNIHTPVSRPNRGFFYRLFRRGGCLTMVPSEKEVEPKQC---------- 578
GRK5    GRL..AEYEV..RLEAGMLD..PPDLNRN-HPPEP-PKKGLLQRLFKRQHQNNSKSSPSSKTSFNHHINSNHVSSNSTGSS 590
```

Figure 5 Interdomain contacts of the C-terminus of GRK6. (**A**) The αCT helix docks between the bundle lobe of the RH domain and the αJ region of the C-tail. Residues preceding αCT wind through the cleft between the bundle and terminal lobes of the RH domain. The fact that this region is well ordered and dependent on the open conformation of GRK6 suggests that the C-terminus of GRK6 helps to stabilize the closed state of the kinase domain. The last observed residue, Ser557, is four residues before a cysteine-rich sequence that is known to be palmitoylated *in vivo* (see panel **E**). Of these cysteines, acylated Cys565 would be most capable of interacting with the membrane in our model of membrane-bound GRK6 (Figure 6). It is possible that additional conformational changes could occur in GRK6 as a consequence of GPCR binding that would bring Cys561 and Cys562 into closer proximity with the membrane plane. However, these post-translational modifications may serve purposes other than membrane binding in the active state of GRK6 (see text and Figure 6). (**B**) The loop that precedes αCT forms an unusual structure with two tight turns that also helps to coordinate a sulphate anion. Pro546 was modelled with a *cis*-peptide bond. (**C**) Interactions between hydrophobic residues in αCT and the side chains of Arg455, Ala458, and Met460 from the C-tail, and Val92 from the bundle lobe of the RH. All of these residues are conserved in the GRK4 subfamily (see panel **E**). (**D**) Conserved salt bridges formed among residues in αCT and the RH domain. Mutation of Arg554 or of the hydrophobic residues in αCT (panel **C**) led to significantly reduced activity in GRK5 (Thiyagarajan *et al*, 2004). (**E**) Sequence alignment of human GRK4 subfamily members, highlighting conserved residues involved in contacts at the C-terminus. Residues involved in apolar contacts are coloured magenta, and acidic and basic residues involved in salt bridges are coloured red and blue, respectively. Asterisks mark the residues that are known (GRK6) or anticipated (GRK4) to be palmitoylated (Stoffel *et al*, 1994; Premont *et al*, 1996).

shape and electrostatic properties to the activated GPCR in its membrane environment. In the case of GRK6, this complementary surface includes the αNT/C-tail region and the adjacent basic membrane-binding surface (Figures 3 and 6). Thus, GRKs simply have to search for a complementary surface to recognize and specifically phosphorylate a broad range of sequence-diverse, but active, receptors.

An assumption in interpreting our mutagenesis experiments was that GRK6 adopts the same closed conformation whether it is phosphorylating a peptide or a receptor. The fact that truncations of the N-terminus of GRKs are deficient in peptide phosphorylation (Huang *et al*, 2009) suggests that αNT forms similar interactions to stabilize the closed state with either receptor or peptide substrate, and consequently that the open and closed states of GRKs are in equilibrium, with the open, inactive state being favoured in solution (Huang *et al*, 2009). GPCR and phospholipid binding could facilitate catalysis by simply driving the equilibrium towards the closed state. Peptides derived from the N-terminus of GRKs are not helical in solution (Pao *et al*, 2009), and this region is disordered in all but one prior GRK structure. Thus, it seems likely that the free energy of GPCR binding helps to constrain the αNT region in a helical conformation that can better interact with and stabilize the closed conformation of the kinase domain. Regardless of the precise mechanism, it is clear from our data that receptor/membrane binding, as mediated by the αNT helix and the adjacent basic region of GRK6, is intimately coupled with allosteric activation, because the GPCR docking site can only form in the closed state of the GRK.

The N-terminus and C-tail were not the only structural elements to become ordered in the closed conformation of GRK6. Surprisingly, an additional 22 amino acids of the C-terminus of GRK6 were also resolved and interact with the RH and kinase domains using residues that are highly conserved in the GRK4 subfamily and that are known to influence kinase activity (Figure 5). The observed C-terminal structure would place the palmitoylation sites of GRK6

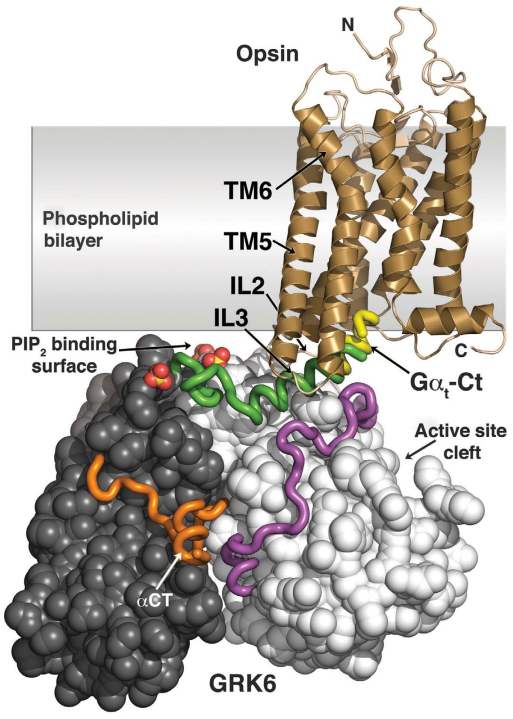

Figure 6 Hypothetical model of GRK6 bound to opsin. The side chains of three exposed hydrophobic residues in αNT (Leu3, Ile6, and Leu7) were aligned with the side chains of three residues in the $G\alpha_t$–Ct peptide bound to opsin (Leu344, Leu341, and Ile340, respectively) (PDB entry 3DQB). In the resulting complex, the proposed phospholipid-binding surface of GRK6 (Figure 3) is brought in close proximity to the expected plane of the phospholipid bilayer as positioned by the opsin structure, and the αNT helix packs between the second and third intracellular loops (IL2 and IL3) of the receptor. GRKs that have additional residues at the N-terminus (e.g. GRK1, which has three more than GRK6, see Figure 2C) can still be accommodated by the large cleft between IL3 and the C-terminus of the receptor. Furthermore, in this model either a longer IL3 loop (as is common in other GPCRs) or the cytoplasmic tail of rhodopsin (which extends an additional 22 amino acids beyond the last ordered residue in this model) can readily access the kinase active site cleft and serve as phosphoacceptors. As modelled, αNT does not penetrate as far into the core of the receptor as the $G\alpha_t$–Ct peptide, which may help explain the relative lack of selectivity of GRKs for specific GPCRs compared with Gα subunits. It should be emphasized, however, that this GRK6–opsin complex is at best a low-resolution model because opsin is not a fully activated receptor, and the GRK6 model is close to, but not yet in a fully closed conformation. There are also other regions besides αNT that are likely involved in interactions with GPCRs, such as residues that would come into contact with IL1 and IL2.

(which are not conserved among GRKs) relatively far from the predicted membrane plane (Figure 6), implying that the GRK6 C-terminus has a function in stabilizing the closed, receptor-bound state of GRK6. If so, the GRK6 C-terminus function similarly to the C-terminal PH domain of GRK2, which binds to Gβγ subunits. The GRK2–Gβγ interaction is essential for membrane translocation of GRK2 in cells, stimulates *in vitro* activity up to 10-fold, and protects the kinase domain of GRK2 against proteolysis (Lodowski *et al*, 2005). A dual function for a lipid-modified domain is not without precedence among AGC kinases. In PKA, N-terminal myristoylation enhances not only membrane association, but also structural stability (Yonemoto *et al*, 1993). The myristoyl group was in fact shown to pack in a hydrophobic pocket formed between its N-terminal helix and the large lobe of the kinase domain (Zheng *et al*, 1993).

In summary, our studies have revealed a unique allosteric mechanism for the activation of an AGC kinase—one that may ultimately afford new opportunities for the selective targeting of GRKs by therapeutic agents. Further confirmation of this model awaits analogous studies in other GRK subfamilies and the structure determination of a GRK–GPCR complex.

Materials and methods

Materials

Sangivamycin was purchased from Berry and Associates, Inc. (Dexter, MI) and (2R,3R)-(-)-2,3-butanediol (97%) was purchased from Sigma-Aldrich.

Protein purification

GRK6 (pal^- mutant) was purified as described previously (Lodowski *et al*, 2006). GRK6 elutes as two peak fractions at ~145 mM (peak 1) and 160 mM NaCl (peak 2) from the Source S column. Crystals could be grown with protein from either peak under similar conditions.

Crystallization

Crystals of GRK6 (peak 1) were grown at 4°C by hanging drop vapour diffusion method by mixing 1 μl protein solution with 1 μl of well solution. GRK6 (10 mg/ml) pre-mixed with 400 μM sangivamycin (in DMSO) and 200 μM $MgCl_2$ was used for crystallization trials. Crystals were grown with well solution consisting of 1.9 M ammonium sulphate and 100 mM Bis–Tris pH 5.2. Rod-like plates appeared within a few days and grew to maximum dimensions of $500 \times 50 \times 5$ μm in a week. For cryoprotection, crystals were soaked in a solution consisting of 2.2 M ammonium sulphate, 100 mM Bis–Tris pH 5.2, 20 mM HEPES pH 8, 200 mM NaCl, 2 mM DTT, 400 μM sangivamycin, 200 μM $MgCl_2$, and 20% (2R,3R)-(-)-butanediol. Crystals could also be obtained under similar conditions by co-crystallization with AMP. For these, hanging drops contained 10 mg/ml GRK6, 4 mM AMP pH 7.5, and 2 mM $MgCl_2$ mixed in a 1:1 ratio with a well solution containing 1.6 M ammonium sulphate and 100 mM Bis–Tris pH 5.2. The AMP crystals were cryo-protected in a solution consisting of 1.8 M ammonium sulphate, 100 mM Bis–Tris pH 5.2, 20 mM HEPES pH 8, 200 mM NaCl, 2 mM DTT, 4 mM AMP pH 7.5, 2 mM $MgCl_2$, and 20% (2R,3R)-(-)-2,3-butanediol. We were unable to grow crystals in the presence of ADP or ATP analogues, perhaps because these compounds favour a distinct, more closed conformation of the kinase domain that is incompatible with the lattice of the $P6_1$ crystals.

Data collection and structure determination

Diffraction maxima were collected at LS-CAT beam line 21-ID-G from crystals maintained at 110 K. The HKL2000 software package was used for data reduction, and the structure of GRK6 (2ACX) was used as a molecular replacement search model using *PHASER* (Storoni *et al*, 2004) in the CCP4 suite (Winn, 2003). The model was refined using *REFMAC* (Murshudov *et al*, 1997) alternating with manual model building using O (Jones *et al*, 1991). Owing to the high anisotropy of the data, ellipsoidal truncation of the data, as described in Table I, was performed before scaling with *SCALEPACK*, as described previously (Lodowski *et al*, 2003). Truncation lead to 2–3% reduction in working and free R-factors compared with untruncated data, significantly improved the quality of the electron density maps, and allowed the modelling of some solvent molecules. Non-crystallographic symmetry restraints were imposed on the two chains in the asymmetric unit throughout refinement. The stereochemistry of the model was evaluated using *PROCHECK* (Laskowski *et al*, 1993). The final refinement statistics are summarized in Table I, and the final structure spans residues 2–557 (out of 576 total), with only residues 387–389 missing in the αF-αG loop and 19 residues missing from the extreme C-terminus. As in the previously reported GRK6·AMPPNP and GRK1 structures (Lodowski *et al*, 2006; Singh *et al*, 2008), GRK6 crystallized as a

non-physiological domain-swapped dimer, with the swap involving residues at the extreme C-terminus. Both subunits in the asymmetric unit of the crystals are essentially identical and exist in similar packing environments. Indeed, some datasets collected clearly belong to a higher symmetry space group ($P6_122$) with one chain per asymmetric unit. The electron density maps were all consistent with the N-terminal methionine being cleaved and the second residue *N*-acetylated, as has been confirmed for other GRKs expressed in ovarian insect cells (Pitcher *et al*, 1999; Singh *et al*, 2008). Final coordinates and structure factors are deposited in the Protein Data Bank as entries 3NYN and 3NYO for the sangivamycin and AMP complexes, respectively.

ROS and peptide phosphorylation assays

We used the GRK6C splice variant (Figure 5E) for kinetic assays because it has higher reported activity towards bROS than other splice forms (Vatter *et al*, 2005). cDNA coding for human GRK6C with a non-cleavable hexa-histidine tag at the C-terminus was cloned into the *Bam*HI and *Eco*RI sites downstream of the polyhedrin promoter in the pFastBac Dual vector (Invitrogen) to create pFastBac-GRK6C-H_6. Site-specific mutants were introduced using the QuikChange Site-Directed Mutagenesis kit (Stratagene) and all sequences were verified by DNA sequencing. Recombinant protein was purified from high five insect cells as described previously for GRK6-531-H_6 (Huang *et al*, 2009). For bROS phosphorylation, steady-state kinetics were conducted at saturating ATP (0.5 mM) using 10–60 μM (80 μM in the case of wild-type GRK6C) urea-washed bROS and 0.3–5 μM GRK mutants in 100 mM HEPES-NaOH pH 7.5, 0.15 M NaCl, 10 mM $MgCl_2$, and 1 mM EDTA (Buffer A). The reaction was initiated by addition of ATP and then incubated at room temperature (22–26°C). We used relatively high ionic strength (150 mM NaCl) in our reactions because we wished to more closely emulate physiological conditions. For peptide C phosphorylation, the reactions contained 0.9–10 μM GRK variant, 500 μM ATP, and 0.23–4 mM peptide in Buffer A.

Acknowledgements

We thank the laboratory of Dr Krzysztof Palczewski for supplying bROS. Work was supported by NIH grants HL071818 and HL086865 (to JT). This research used the Cell and Molecular Biology Core of the Michigan Diabetes Research and Training Center supported by DK20572. Use of LS-CAT Sector 21 was supported by the Michigan Economic Development Corporation and the Michigan Technology Tri-Corridor (Grant 085P1000817). Use of the Advanced Photon Source was supported by the US Department of Energy, Office of Science, Office of Basic Energy Sciences, under contract no. DE-AC02-06CH11357.

Conflict of interest

The authors declare that they have no conflict of interest.

References

Chen CK, Inglese J, Lefkowitz RJ, Hurley JB (1995) Ca^{2+}-dependent interaction of recoverin with rhodopsin kinase. *J Biol Chem* **270:** 18060–18066

Chen CY, Dion SB, Kim CM, Benovic JL (1993) β-adrenergic receptor kinase. Agonist-dependent receptor binding promotes kinase activation. *J Biol Chem* **268:** 7825–7831

Dorn II GW (2009) GRK mythology: G-protein receptor kinases in cardiovascular disease. *J Mol Med* **87:** 455–463

Huang CC, Yoshino-Koh K, Tesmer JJ (2009) A surface of the kinase domain critical for the allosteric activation of G protein-coupled receptor kinases. *J Biol Chem* **284:** 17206–17215

Jones TA, Zou JY, Cowan SW, Kjeldgaard M (1991) Improved methods for the building of protein models in electron density maps and the location of errors in these models. *Acta Crystallogr A* **47:** 110–119

Kannan N, Haste N, Taylor SS, Neuwald AF (2007) The hallmark of AGC kinase functional divergence is its C-terminal tail, a cis-acting regulatory module. *Proc Natl Acad Sci USA* **104:** 1272–1277

Kim CM, Dion SB, Benovic JL (1993) Mechanism of β-adrenergic receptor kinase activation by G proteins. *J Biol Chem* **268:** 15412–15418

Laskowski RA, MacArthur MW, Moss DS, Thornton JM (1993) PROCHECK: a program to check the stereochemical quality of protein structures. *J Appl Crystallogr* **26:** 283–291

Lodowski DT, Barnhill JF, Pyskadlo RM, Ghirlando R, Sterne-Marr R, Tesmer JJ (2005) The role of Gβγ and domain interfaces in the activation of G protein-coupled receptor kinase 2. *Biochemistry* **44:** 6958–6970

Lodowski DT, Pitcher JA, Capel WD, Lefkowitz RJ, Tesmer JJ (2003) Keeping G proteins at bay: a complex between G protein-coupled receptor kinase 2 and Gβγ. *Science* **300:** 1256–1262

Lodowski DT, Tesmer VM, Benovic JL, Tesmer JJ (2006) The structure of G protein-coupled receptor kinase (GRK)-6 defines a second lineage of GRKs. *J Biol Chem* **281:** 16785–16793

Loomis CR, Bell RM (1988) Sangivamycin, a nucleoside analogue, is a potent inhibitor of protein kinase C. *J Biol Chem* **263:** 1682–1692

Madhusudan, Akamine P, Xuong NH, Taylor SS (2002) Crystal structure of a transition state mimic of the catalytic subunit of cAMP-dependent protein kinase. *Nat Struct Biol* **9:** 273–277

McCarthy NE, Akhtar M (2002) Activation of rhodopsin kinase. *Biochem J* **363** (Part 2)**:** 359–364

Metaye T, Gibelin H, Perdrisot R, Kraimps JL (2005) Pathophysiological roles of G-protein-coupled receptor kinases. *Cell Signal* **17:** 917–928

Murshudov GN, Vagin AA, Dodson EJ (1997) Refinement of macromolecular structures by the maximum-likelihood method. *Acta Crystallogr D Biol Crystallogr* **53** (Part 3)**:** 240–255

Noble B, Kallal LA, Pausch MH, Benovic JL (2003) Development of a yeast bioassay to characterize G protein-coupled receptor kinases. Identification of an NH_2-terminal region essential for receptor phosphorylation. *J Biol Chem* **278:** 47466–47476

Oldham WM, Hamm HE (2006) Structural basis of function in heterotrimeric G proteins. *Q Rev Biophys* **39:** 117–166

Onorato JJ, Palczewski K, Regan JW, Caron MG, Lefkowitz RJ, Benovic JL (1991) Role of acidic amino acids in peptide substrates of the β-adrenergic receptor kinase and rhodopsin kinase. *Biochemistry* **30:** 5118–5125

Palczewski K, Buczylko J, Kaplan MW, Polans AS, Crabb JW (1991) Mechanism of rhodopsin kinase activation. *J Biol Chem* **266:** 12949–12955

Palczewski K, Buczylko J, Lebioda L, Crabb JW, Polans AS (1993) Identification of the N-terminal region in rhodopsin kinase involved in its interaction with rhodopsin. *J Biol Chem* **268:** 6004–6013

Palczewski K, Kahn N, Hargrave PA (1990) Nucleoside inhibitors of rhodopsin kinase. *Biochemistry* **29:** 6276–6282

Pao CS, Barker BL, Benovic JL (2009) Role of the amino terminus of G protein-coupled receptor kinase 2 in receptor phosphorylation. *Biochemistry* **48:** 7325–7333

Pitcher JA, Fredericks ZL, Stone WC, Premont RT, Stoffel RH, Koch WJ, Lefkowitz RJ (1996) Phosphatidylinositol 4,5-bisphosphate (PIP_2)-enhanced G protein-coupled receptor kinase (GRK) activity. Location, structure, and regulation of the PIP_2 binding site distinguishes the GRK subfamilies. *J Biol Chem* **271:** 24907–24913

Pitcher JA, Freedman NJ, Lefkowitz RJ (1998) G protein-coupled receptor kinases. *Annu Rev Biochem* **67:** 653–692

Pitcher JA, Tesmer JJ, Freeman JL, Capel WD, Stone WC, Lefkowitz RJ (1999) Feedback inhibition of G protein-coupled receptor kinase 2 (GRK2) activity by extracellular signal-regulated kinases. *J Biol Chem* **274:** 34531–34534

Premont RT, Gainetdinov RR (2007) Physiological roles of G protein-coupled receptor kinases and arrestins. *Annu Rev Physiol* **69:** 511–534

Premont RT, Macrae AD, Stoffel RH, Chung N, Pitcher JA, Ambrose C, Inglese J, MacDonald ME, Lefkowitz RJ (1996) Characterization of the G protein-coupled receptor kinase GRK4. Identification of four splice variants. *J Biol Chem* **271:** 6403–6410

Rosenbaum DM, Rasmussen SG, Kobilka BK (2009) The structure and function of G-protein-coupled receptors. *Nature* **459:** 356–363

Scheerer P, Park JH, Hildebrand PW, Kim YJ, Krauss N, Choe HW, Hofmann KP, Ernst OP (2008) Crystal structure of opsin in its G-protein-interacting conformation. *Nature* **455:** 497–502

Singh P, Wang B, Maeda T, Palczewski K, Tesmer JJ (2008) Structures of rhodopsin kinase in different ligand states reveal key elements involved in G protein-coupled receptor kinase activation. *J Biol Chem* **283:** 14053–14062

Sterne-Marr R, Leahey PA, Bresee JE, Dickson HM, Ho W, Ragusa MJ, Donnelly RM, Amie SM, Krywy JA, Brookins-Danz ED, Orakwue SC, Carr MJ, Yoshino-Koh K, Li Q, Tesmer JJ (2009) GRK2 activation by receptors: role of the kinase large lobe and carboxyl-terminal tail. *Biochemistry* **48:** 4285–4293

Stoffel RH, Randall RR, Premont RT, Lefkowitz RJ, Inglese J (1994) Palmitoylation of G protein-coupled receptor kinase, GRK6. Lipid modification diversity in the GRK family. *J Biol Chem* **269:** 27791–27794

Storoni LC, McCoy AJ, Read RJ (2004) Likelihood-enhanced fast rotation functions. *Acta Crystallogr D Biol Crystallogr* **60** (Part 3)**:** 432–438

Thiyagarajan MM, Stracquatanio RP, Pronin AN, Evanko DS, Benovic JL, Wedegaertner PB (2004) A predicted amphipathic helix mediates plasma membrane localization of GRK5. *J Biol Chem* **279:** 17989–17995

Vatter P, Stoesser C, Samel I, Gierschik P, Moepps B (2005) The variable C-terminal extension of G-protein-coupled receptor kinase 6 constitutes an accessorial autoregulatory domain. *FEBS J* **272:** 6039–6051

Winn MD (2003) An overview of the CCP4 project in protein crystallography: an example of a collaborative project. *J Synchrotron Radiat* **10** (Part 1)**:** 23–25

Yang J, Cron P, Good VM, Thompson V, Hemmings BA, Barford D (2002) Crystal structure of an activated Akt/protein kinase B ternary complex with GSK3-peptide and AMP-PNP. *Nat Struct Biol* **9:** 940–944

Yonemoto W, McGlone ML, Taylor SS (1993) N-myristylation of the catalytic subunit of cAMP-dependent protein kinase conveys structural stability. *J Biol Chem* **268:** 2348–2352

Yu QM, Cheng ZJ, Gan XQ, Bao GB, Li L, Pei G (1999) The amino terminus with a conserved glutamic acid of G protein-coupled receptor kinases is indispensable for their ability to phosphorylate photoactivated rhodopsin. *J Neurochem* **73:** 1222–1227

Zheng J, Knighton DR, Xuong NH, Taylor SS, Sowadski JM, Ten Eyck LF (1993) Crystal structures of the myristylated catalytic subunit of cAMP-dependent protein kinase reveal open and closed conformations. *Protein Sci* **2:** 1559–1573